Dynamical Degeneracy Splitting and Directional Invisibility in Non-Hermitian Systems

Kai Zhang,[1] Chen Fang,[1,2,3,*] and Zhesen Yang[3,4,†]
[1]Beijing National Laboratory for Condensed Matter Physics, and Institute of Physics, Chinese Academy of Sciences, Beijing 100190, China
[2]Songshan Lake Materials Laboratory, Dongguan, Guangdong 523808, China
[3]Kavli Institute for Theoretical Sciences, Chinese Academy of Sciences, Beijing 100190, China
[4]Department of Physics, Xiamen University, Xiamen 361005, Fujian Province, China

(Received 22 November 2022; revised 28 February 2023; accepted 21 June 2023; published 20 July 2023)

In this Letter, we introduce the concept of dynamical degeneracy splitting to describe the anisotropic decay behaviors in non-Hermitian systems. We demonstrate that systems with dynamical degeneracy splitting exhibit two distinctive features: (i) the system shows frequency-resolved non-Hermitian skin effect; (ii) Green's function exhibits anomalous behavior at given frequency, leading to uneven broadening in spectral function and anomalous scattering. As an application, we propose directional invisibility based on wave packet dynamics to investigate the geometry-dependent skin effect in higher dimensions. Our work elucidates a faithful correspondence between non-Hermitian skin effect and Green's function, offering a guiding principle for exploration of novel physical phenomena emerging from this effect.

DOI: 10.1103/PhysRevLett.131.036402

Introduction.—Non-Hermitian Hamiltonians [1–6], which can effectively capture the dynamics of the system that is coupled to external environments, have been implemented in a wide variety of systems [7–19]. Without the constraint of Hermiticity, the eigenvalues of the Hamiltonian can be complex, leading to many intriguing phenomena in non-Hermitian systems. One such phenomenon is the non-Hermitian skin effect (NHSE) [20–64], which refers to that extensive eigenstates of system-size order are concentrated on the open boundaries; and that the energy spectrum is highly sensitive to the change of boundary conditions. In one dimension, the NHSE can be well understood within the framework of the non-Bloch band theory [20,21,24,36]. Extending to higher dimensions, several new appearances in NHSE have been discovered [28,40,57,58] and the generalization of the non-Bloch theory has also been attempted [22,65–67]. However, to date, many questions still need to be solved. One representative is the recently discovered geometry-dependent skin effect [58], where the appearance of NHSE clearly depends on the geometric shapes of the open boundary. How do we interpret and find a guiding principle to detect such kinds of phenomena in higher dimensions? This is one motivation for this work.

Another motivation comes from the following considerations. Previous studies have suggested that the spectral area of the Bloch spectrum can faithfully predict the presence of higher-dimensional NHSE [58]; however, this criterion loses the information of band structures around a given frequency $\omega \in \mathbb{R}$ [68], which is primarily concerned in spectroscopic measurements [69]. Moreover, the criterion fails to relate NHSE to realistic physical observations. For example, in condensed matter physics, the transport and response properties of the system are mainly determined by the excitations near the Fermi energy; thus, only NHSE appearing near the Fermi energy does matter, which cannot be inferred from the spectral-area criterion. These considerations inspire us to find a frequency criterion for the manifestation of NHSE, thereby delivering NHSE to broader physical scenarios.

In this Letter, we demonstrate that the dynamical degeneracy splitting plays the role of frequency criterion for the appearance of NHSE. From the perspective of bulk-boundary correspondence, the dynamical degeneracy splitting reflects the bulk characteristic of the NHSE and is independent of boundary conditions, which implies that the dynamical degeneracy splitting may be more intrinsic than the NHSE itself. As illustrated in Fig. 1(a), the dynamical degeneracy splitting not only helps us to understand the physical origin of NHSE, but also reveal a deep relation to the Green's function. Given this connection, we establish the scattering theory in non-Hermitian systems, and reveal that when the dynamical degeneracy splitting occurs, the scattered waves will be damped away from impurities. Applying the scattering theory to geometry-dependent skin effect, we propose a new phenomenon unique to non-Hermitian systems called directional invisibility, which refers to the fact that the reflected components of the incident wave packet are visible when the impurity line is in several spatial directions but invisible in the remaining directions. As an application, directional invisibility can serve as an experimentally feasible method to directly detect the existence of geometry-dependent skin effect without the need for open boundary conditions.

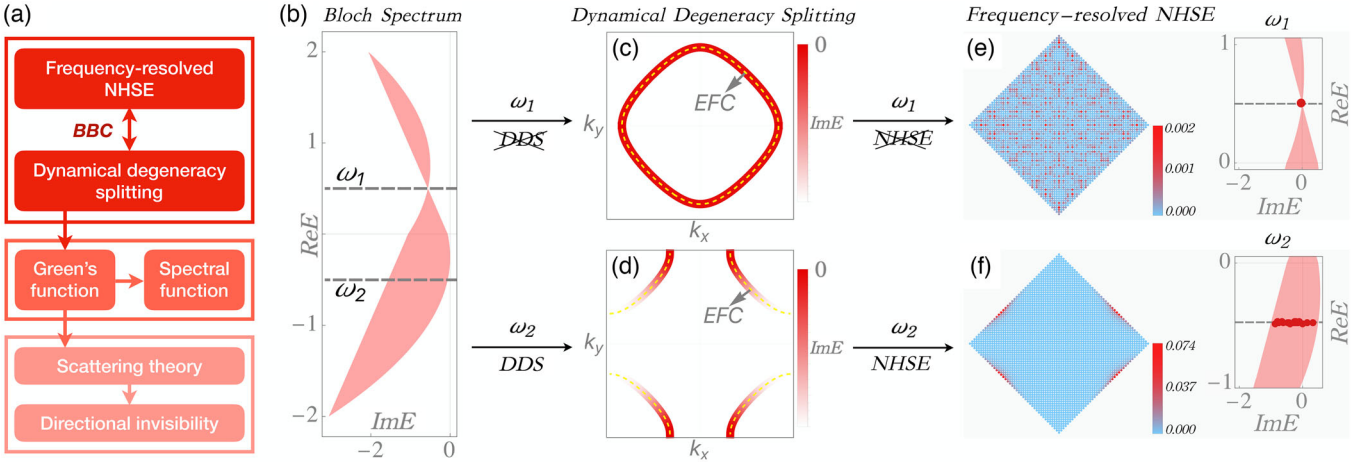

FIG. 1. (a) Schematic of the relation between dynamical degeneracy splitting (DDS), frequency-resolved NHSE, and the physical consequences via Green's function. (b)–(f) show the bulk-boundary correspondence between dynamical degeneracy splitting and frequency-resolved NHSE. For the Bloch spectrum in (b), there is no dynamical degeneracy splitting at excitation frequency ω_1 in (c), where the color bar corresponds to imaginary energy $\mathrm{Im}E(\boldsymbol{k})$ on the equal-frequency contour (the dashed yellow lines). Correspondingly, NHSE is absent at this frequency in (e). Dynamical degeneracy splitting occurs at ω_2 as shown in (d), and consequently, NHSE appears at frequency ω_2 in (f).

Dynamical degeneracy splitting and frequency-resolved NHSE.—Now we start with the non-Hermitian Bloch band $E_\mu(\boldsymbol{k})$ to explain what dynamical degeneracy splitting is. For a given excitation frequency $\omega \in \mathbb{R}$ (the real frequency is assumed throughout this Letter), the equal-frequency contour $\boldsymbol{K}(\omega)$ can be defined as

$$\boldsymbol{K}(\omega \in \mathbb{R}) = \boldsymbol{K}_1(\omega \in \mathbb{R}) \cup \cdots \cup \boldsymbol{K}_m(\omega \in \mathbb{R}), \quad (1)$$

where $\boldsymbol{K}_\mu(\omega \in \mathbb{R}) = \{\boldsymbol{k} \in \mathrm{BZ} | \mathrm{Re}E_\mu(\boldsymbol{k}) = \omega\}$ and BZ is short for Brillouin zone. When ω is chosen to be the chemical potential in electronic systems, $\boldsymbol{K}(\omega)$ is nothing but the renormalized Fermi surface. An example is illustrated in Figs. 1(b)–1(d). When $\omega = \omega_1$ or ω_2, the corresponding equal-frequency contour is plotted in Figs. 1(c) or 1(d) by the yellow dashed lines. Physically, each point on the equal-frequency contour in Fig. 1(c) corresponds to an excited mode at frequency ω_1, and the corresponding group velocity of this mode in real space is along the normal direction at that point on the equal-frequency contour [70].

In the Hermitian case, all excited modes at frequency ω are degenerate since $\mathrm{Im}E_\mu(\boldsymbol{k}) = 0$ for all $\boldsymbol{k}$. Under a generic open boundary geometry, the corresponding eigenstate with energy ω is constructed by the linear superposition of these $\boldsymbol{k} \in \boldsymbol{K}(\omega)$. However, once the non-Hermitian term is introduced, the imaginary part $\mathrm{Im}E_\mu(\boldsymbol{k})$ will broaden the equal-frequency contour in complex ways, which in general will split this degeneracy as shown in Fig. 1(d). As a result, even under the same open boundary geometry, the original linear superposition of Bloch waves is no longer to be the eigenstate, which implies the emergence of NHSE at frequency ω [70]. We refer to the above type of degeneracy splitting as dynamic degeneracy splitting. This phenomenon results from differences in the lifetimes of equal-frequency excitation modes, has a dynamical consequence, and corresponds to the frequency-resolved NHSE.

We use the example $H_{\mathrm{NH}}(\boldsymbol{k}) = \cos k_x + \cos k_y + i[(1/2 - \cos k_x - \cos k_y)\cos k_x] - i9/16$ to demonstrate this point. As shown in Fig. 1(b), the dynamical degeneracy splitting occurs at $\omega_2 = -1/2$ but not $\omega_1 = 1/2$. It implies that these eigenstates $\psi_{i\in\omega_2(\omega_1)}(\boldsymbol{r})$ with eigenvalues satisfying $\mathrm{Re}\, E_{i,\mathrm{OBC}} = \omega_2(\omega_1)$ will show (not show) NHSE at this frequency. In Figs. 1(e) and 1(f), we plot $P_\omega(\boldsymbol{r}) = \sum_{i\in\omega} |\psi_i(\boldsymbol{r})|^2$ on the diamond geometry with lattice size $L_x = L_y = 80$. It is shown that $P_{\omega_1}(\boldsymbol{r})$ is extensive on the entire lattice in (e), but $P_{\omega_2}(\boldsymbol{r})$ shows localization behavior in (f), which demonstrates the correspondence between the dynamical degeneracy splitting and frequency-resolved NHSE.

Dynamical degeneracy splitting in Green's function.—Apart from the relation to NHSE, dynamical degeneracy splitting is also associated with Green's function as illustrated in Fig. 1(a). One consequence from dynamical degeneracy splitting is the uneven broadening in the spectral function at the excitation frequency ω. For a given non-Hermitian Hamiltonian $H_{\mathrm{NH}}(\boldsymbol{k})$, one can calculate the spectral function $A(\omega, \boldsymbol{k}) = -\mathrm{Im}\mathrm{Tr}\{1/[\omega + i\eta - H_{\mathrm{NH}}(\boldsymbol{k})]\}$ to characterize the dynamical degeneracy splitting, which can be measured directly, for example, by the angle-resolved photoemission spectroscopy. Therefore, one can identify the dynamical degeneracy splitting from the experimental side by observing the nonuniform broadening of equal-frequency contour under a given excitation frequency. Applying this result to condensed matter physics, we further propose that quasiparticle interference become anomalous as discussed in [70]. This will be another

experimental signature for the existence of dynamical degeneracy splitting.

Next, we will demonstrate that anomalous scattering behavior is another consequence of dynamical degeneracy splitting via Green's function. The anomalous scattering here refers to the phenomenon that a defect can scatter the propagating plane waves to exponentially damped waves away from the scatterer.

Anomalous scattering theory.—We first establish a general scattering theory in a two-dimensional non-Hermitian system with single band. It is straightforward to extend our discussion to general situations [70]. The full Hamiltonian can be expressed as $H = H_{\mathrm{NH}}(\boldsymbol{k}) + V$, where V is the scattering potential. Now, consider an incident wave $\phi_i(\boldsymbol{r})$ (or an excitation) with momentum $\boldsymbol{k}_i$ propagating on the lattice and hitting the scatterer. Then, the scattered waves $\phi_s(\boldsymbol{r})$ can be captured by the following integral equation [70]:

$$\begin{aligned}\psi(\boldsymbol{r}) &= \phi_i(\boldsymbol{r}) + \phi_s(\boldsymbol{r}) \\ &= \phi_{\boldsymbol{k}_i}(\boldsymbol{r}) + \int d\boldsymbol{r}' G_0^+[E(\boldsymbol{k}_i);\boldsymbol{r},\boldsymbol{r}']\mathcal{V}(\boldsymbol{r}')\psi(\boldsymbol{r}'), \quad (2)\end{aligned}$$

where $\phi_{\boldsymbol{k}_i}(\boldsymbol{r}) = \langle \boldsymbol{r}|\phi_{\boldsymbol{k}_i}\rangle = e^{i\boldsymbol{k}_i\boldsymbol{r}}$ represents the incident wave, and $\phi_s(\boldsymbol{r})$ comprises reflected and transmitted waves. Here, $\mathcal{V}(\boldsymbol{r}) = \langle \boldsymbol{r}|V|\boldsymbol{r}\rangle$ is the scattering potential function, and $G_0^+[E(\boldsymbol{k}_i);\boldsymbol{r},\boldsymbol{r}'] = \langle \boldsymbol{r}|[E(\boldsymbol{k}_i) + i\eta - H_{\mathrm{NH}}(\boldsymbol{k})]^{-1}|\boldsymbol{r}'\rangle$ with $\eta \to 0^+$ is the retarded Green's function. The integral equation Eq. (2) tells us that (i) after introducing the scattering potential V, the eigenstate of the full Hamiltonian H, i.e., $\psi(\boldsymbol{r})$, can be decomposed into the incident and scattered waves with the same energy $E(\boldsymbol{k}_i)$ [70]; (ii) the anomalous behavior of the scattering process comes from the anomalous property of the retarded Green's function in non-Hermitian systems.

Now we use an impurity line, labeled by $\mathcal{L}_\theta$, as an example to demonstrate the anomalous scattering. As shown in Figs. 2(a) and 2(b), we specify the impurity line lying on the position $r_\perp = 0$ and along the θ direction. For the left (right) side of the impurity line $\mathcal{L}_\theta$, the corresponding region is denoted by $r_\perp < 0$ ($r_\perp > 0$). Therefore, the impurity-line scattering potential function reads

$$\mathcal{V}(\boldsymbol{r}) = \lambda\delta(r_\perp = 0). \quad (3)$$

Note that the translation symmetry along the r_θ direction is preserved in the scattering process. Therefore, we substitute Eq. (3) into Eq. (2) and take the Fourier transform from r_θ to k_θ, and finally obtain the solution of scattering wave [70] as

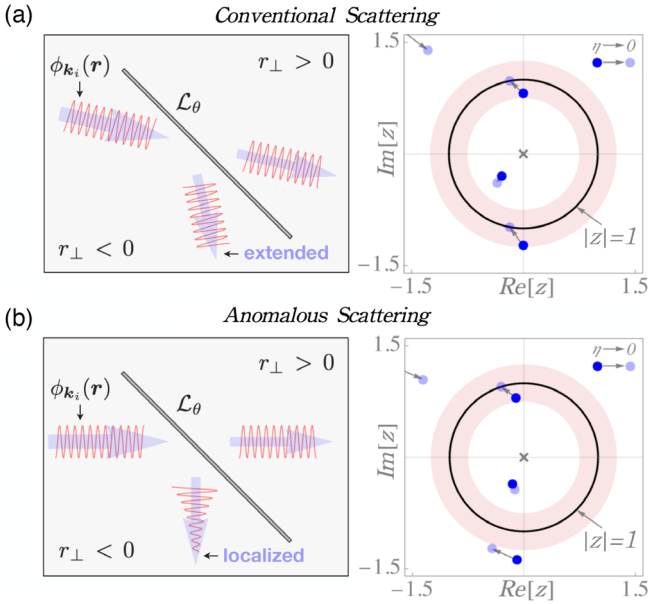

FIG. 2. The illustrations of conventional scattering in (a) and anomalous scattering in (b). Here, the model Hamiltonian reads $H_{\mathrm{NH}}(\boldsymbol{k}) = 2\sin k_x \cos k_y - 2\cos k_x + i(\cos k_x - 1)$, and the impurity line $\mathcal{L}_\theta$ is along the $\theta = 3\pi/4$ direction. The dark and light blue dots represents parts of poles calculated in Eq. (4). As $\eta \to 0$, the corresponding poles evolve from dark to light blue dots, as indicated by arrows.

$$\phi_s(k_i^\theta, r_\perp) = \lambda\psi(k_i^\theta, 0)\begin{cases}\sum\limits_{|z_{\mathrm{in}}|<1} C(z_{\mathrm{in}}) z_{\mathrm{in}}^{r_\perp}, & r_\perp > 0; \\ \sum\limits_{|z_{\mathrm{out}}|>1} -C(z_{\mathrm{out}}) z_{\mathrm{out}}^{r_\perp}, & r_\perp < 0,\end{cases} \quad (4)$$

where $k_i^\theta = \boldsymbol{k}_i \cdot \boldsymbol{e}_\theta$ is the θ component of the incident momentum; the coefficient $\psi(k_i^\theta, 0)$ is a constant for a given k_i^θ; $C(z_{\mathrm{in-out}})$ equals $2\pi i$ times the residue of the function $[z[E(\boldsymbol{k}_i) + i\eta - H_{\mathrm{NH}}(k_i^\theta, z)]]^{-1}$ at the poles z_{in} and z_{out} inside and outside the $|z| = 1$ curve, respectively, as shown in Figs. 2(a) and 2(b).

Now we show that when the dynamical degeneracy splitting occurs, the reflected wave will become localized. Without loss of generality, we assume the incident plane wave $\boldsymbol{k}_i = (k_i^\theta, k_i^\perp)$ with energy $E(\boldsymbol{k}_i)$ comes from the $r_\perp < 0$ region. There are two cases of scattered waves. In case (i), there are at least two poles that touch the $|z| = 1$ simultaneously from the inner and outer sides, respectively, when $\eta \to 0^+$, and one example is illustrated in Fig. 2(a). In case (ii), there is only one pole that touches the $|z| = 1$ curve from the inside as $\eta \to 0^+$, as shown in Fig. 2(b). More details are present in [70]. It can be seen from Eq. (4) that there will be two dominant propagating modes that survive at infinity for case (i), namely the transmitted wave in the region $r_\perp > 0$ and the reflected wave in the region $r_\perp < 0$, as illustrated in Fig. 2(a). In case (ii), we have one dominant transmitted wave in the $r_\perp > 0$ region, while in

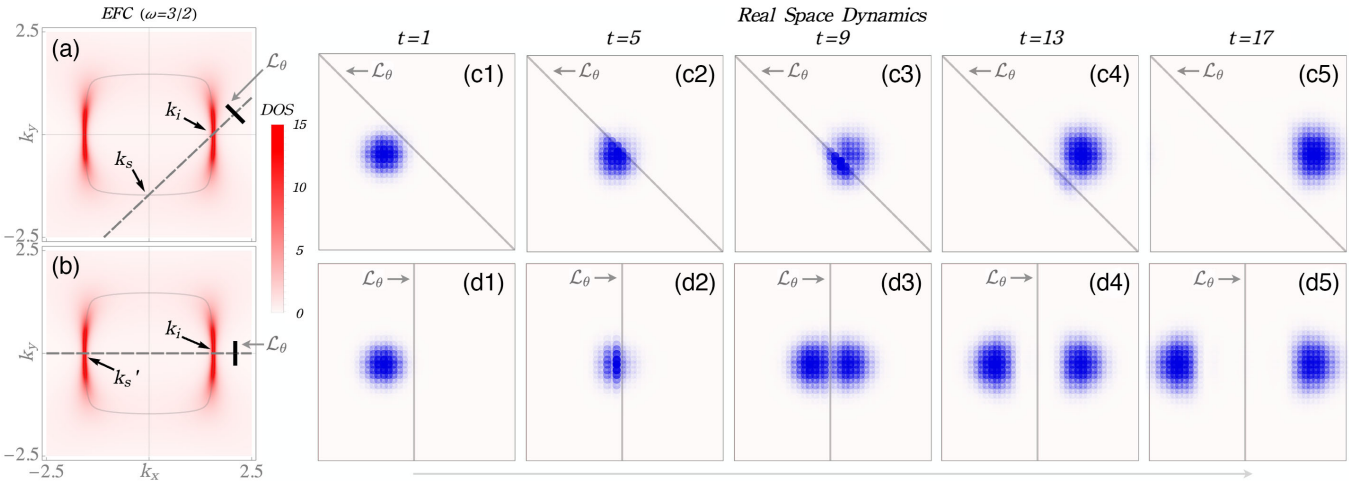

FIG. 3. Directional invisibility in Hamiltonian Eq. (5) with the parameters $(\mu_0, \mu_z, t_0, t, t_z, \gamma) = (1.35, -0.05, -0.4, 0.4, -0.6, 1)$. (a),(b) show the spectral function $A(\omega, \boldsymbol{k})$ with $\omega = 3/2$, of which the intensity corresponds to the opacity as shown in the color bar. Here, $\mathcal{L}_\theta$ represents the impurity line, and $\boldsymbol{k}_i$ denotes the incident wave and $\boldsymbol{k}_s$ ($\boldsymbol{k}_s'$) indicates the scattered wave. The incident wave packet with the momentum center at $\boldsymbol{k}_i$ hits the oblique impurity line in (c1)–(c5) and vertical impurity line in (d1)–(d5), where the impurity strength $\lambda = 1$.

the $r_\perp < 0$ region the dominant reflected wave is a spatially localized wave as $\eta \to 0^+$. Therefore, the scattering process is anomalous, as illustrated in Fig. 2(b).

Directional invisibility.—Now we show that for the geometry-dependent skin effect (GDSE), the corresponding scattering process exhibits directional invisibility. The Bloch Hamiltonian of the GDSE model [58] reads

$$H(\boldsymbol{k}) = \sum_{i=0,x,y,z} d_i(\boldsymbol{k})\sigma_i - \frac{i\gamma}{2}(\sigma_0 - \sigma_z), \tag{5}$$

where $d_i(\boldsymbol{k})$ is a real function of $\boldsymbol{k}$ and σ_i represents the Pauli matrix. The only non-Hermitian parameter $\gamma > 0$ is used to describe the dissipative system. Specifically, $\{d_0, d_x, d_y, d_z\} = \{\mu_0 + t_0(\cos k_x + \cos k_y), t[1 - \cos k_x - \cos k_y + \cos(k_x - k_y)], t[\sin k_x - \sin k_y - \sin(k_x - k_y)], \mu_z + t_z(\cos k_x - \cos k_y)\}$. We plot the spectral function $A(\omega_0, \boldsymbol{k})$ in Figs. 3(a) and 3(b). It shows the uneven broadening on the equal-frequency contour (the gray curve representing equal-frequency contour), which is a definite signature of the occurrence of dynamical degeneracy splitting. According to the established scattering theory, the anomalous scattering will occur.

We assume an incident plane wave has $\boldsymbol{k}_i = (k_i^x, k_i^y) = (\pi/2, 0)$ and hits the impurity line $\mathcal{L}_\theta$ with a rightward velocity in real space. Note that $\boldsymbol{k}_i$ lies on the equal-frequency contour, i.e., $\boldsymbol{K}(\omega)$ with $\omega = 3/2$, as shown in Figs. 3(a) and 3(b). The impurity line $\mathcal{L}_\theta$ preserves the momentum along this direction, which means that the scatterer $\mathcal{L}_\theta$ relates $\boldsymbol{k}_i$ with $\boldsymbol{k}_s$ and $\boldsymbol{k}_s'$ in the way illustrated in Figs. 3(a) and 3(b), respectively. In Fig. 3(a), due to the larger broadening at $\boldsymbol{k}_s$ than that at $\boldsymbol{k}_i$, the reflected wave is damped exponentially away from the impurity line, which means that anomalous scattering occurs as discussed in case (ii). The band dispersion of the Hamiltonian in Eq. (5) is mirror symmetric under $\mathcal{M}_x$: $(k_x, k_y) \to (-k_x, k_y)$ and $\mathcal{M}_y$: $(k_x, k_y) \to (k_x, -k_y)$. This means $\boldsymbol{k}_s' = \mathcal{M}_x\boldsymbol{k}_i$ has the equal broadening with $\boldsymbol{k}_i$, as shown in Fig. 3(b). Therefore, the conventional scattering discussed in case (i) occurs for the vertical impurity line that scatters the incident plane wave to another propagating plane wave $\boldsymbol{k}_s'$. This phenomenon that the visibility of reflected waves depends on the direction of impurity line is dubbed directional invisibility and unique to higher-dimensional non-Hermitian systems.

To probe the directional invisibility in this example, the incident wave is chosen as a Gaussian wave packet with momentum center at $\boldsymbol{k}_i$ for the scattering simulation, as shown in Figs. 3(c) and 3(d). The time evolution of wave packet follows $|\psi(t)\rangle = \mathcal{N}(t)e^{-iHt}|\phi_0\rangle$, where H is the full Hamiltonian consisting of the free Hamiltonian in Eq. (5) and impurity-line scattering potential $\mathcal{V}(\boldsymbol{r}) = \lambda\sigma_0\delta(r_\perp = 0)$, and $\mathcal{N}(t)$ is the normalization factor at every time. The incident Gaussian wave packet has the form $\phi_0(\boldsymbol{r}) = \exp[-(\boldsymbol{r} - \boldsymbol{r}_0)^2/\sigma^2 + i\boldsymbol{k}_i^0\boldsymbol{r}](1, 1)^T$. In Figs. 3(c) and 3(d), the parameters are set as $(x_0, y_0, \sigma) = (14, 20, 4)$, and the lattice size is $L_x = L_y = 40$. It can be observed that the Gaussian wave packet is almost completely transmitted through the oblique impurity line $\mathcal{L}_\theta$ without evident reflected waves, as shown in Figs. 3(c1)–3(c5). However, parts of the wave packet are reflected by the vertical impurity line $\mathcal{L}_\theta$ as a propagating wave, shown in Figs. 3(d1)–3(d5). Therefore, the wave-packet scattering simulation in Figs. 3(c) and 3(d) verifies the directional invisibility.

The role of symmetry.—Now we discuss the role of symmetry, which reveals the correspondence between directional invisibility and GDSE. For $H_{\mathrm{NH}}(\boldsymbol{k})$, all symmetries preserving the complex energy form the scattering group of $H_{\mathrm{NH}}(\boldsymbol{k})$, labeled by G_s, which includes, for example, the reciprocity $\bar{\mathcal{T}}$ [26] and point-group symmetries, such as rotation, inversion, and mirror symmetry $\mathcal{M}$. Now suppose that there is an incident wave with momentum $\boldsymbol{k}_i$. Under the action of G_s, $\boldsymbol{k}_i$ will be mapped to a set of other points on the BZ with the same energy, that is, $E_\mu(\boldsymbol{k}_i) = E_\mu(g_s\boldsymbol{k}_i)$ with $g_s \in G_s$. Note that $\boldsymbol{k}_i$ and $g_s\boldsymbol{k}_i$ determines a direction crossing them, and we label the impurity line perpendicular to this direction by $\mathcal{L}_{g_s\boldsymbol{k}_i}$. Now we state the conclusion: for the incident wave $\boldsymbol{k}_i$, the scattering process for the impurity line $\mathcal{L}_{g_s\boldsymbol{k}_i}$ is conventional; while for all other directions, the scattering process is not protected by symmetry g_s and is generally anomalous. It should be noted that if $g_s = \mathcal{M}$ or $\bar{\mathcal{T}}\mathcal{M}$, $\mathcal{L}_{g_s\boldsymbol{k}_i}$ is exactly parallel or perpendicular to the mirror line, respectively, and is independent of $\boldsymbol{k}_i$. We label such an impurity line as $\mathcal{L}_{g_s}$. It means that for the impurity line $\mathcal{L}_{g_s}$, the scattering process for all possible incident states is conventional. For example, if $H_{\mathrm{NH}}(\boldsymbol{k})$ preserves $\mathcal{M}_x$ symmetry, then $\mathcal{L}_{\mathcal{M}_x}$ is along the y direction, and the conventional scattering occurs on the impurity line $\mathcal{L}_{\mathcal{M}_x}$ for all possible incident waves.

Now we relate it to the GDSE. For GDSE, if there is an edge parallel to the impurity line $\mathcal{L}_{g_s}$, then the edge shows conventional scattering for all $\boldsymbol{k}_i \in \mathrm{BZ}$, correspondingly, the open boundary eigenstates cannot be localized at that edge. Based on this principle, one can find that if the Hamiltonian has $\mathcal{M}$ and/or $\bar{\mathcal{T}}\mathcal{M}$ symmetry, then open boundary eigenstates can no longer be localized at the edges parallel to $\mathcal{L}_{\mathcal{M}}$ and/or $\mathcal{L}_{\bar{\mathcal{T}}\mathcal{M}}$ under any shape of open boundary geometry.

Conclusions and discussions.—In summary, we introduce the concept of dynamical degeneracy splitting to characterize the nonuniform decay behavior of excited modes at a given frequency. On the one hand, the dynamical degeneracy splitting predicts the frequency-resolved NHSE; on the other hand, it associates with the anomaly in Green's function at a specified frequency, leading to uneven broadening in spectral function and anomalous scattering. As an application, we propose a type of anomalous scattering, directional invisibility, as an experimental indicator of the existence of GDSE.

This work essentially provides a frequency criterion that can further help us understand and define NHSE in the system beyond conventional band theory. For example, in the electronic system with self-energy corrections, the retarded Green function has the form $G(\omega,\boldsymbol{k}) = [\omega - \mathcal{H}_{\mathrm{eff}}(\omega,\boldsymbol{k})]^{-1}$, where the effective Hamiltonian depends on the frequency ω. The dynamical degeneracy splitting can still be well defined, correspondingly, the concept of NHSE can be extended in such systems, which laid the foundation for further studies.

K. Z. thank Kai Sun for the valuable discussion. Z. Y. acknowledges funding support by the National Science Foundation of China (Grant No. NSFC-12104450) and the fellowship of China National Postdoctoral Program for Innovative Talents (Grant No. BX2021300). C. F. acknowledges funding support by the Chinese Academy of Sciences under Grant No. XDB33000000.

*cfang@iphy.ac.cn
†yangzs@ucas.ac.cn

[1] I. Rotter, J. Phys. A **42**, 153001 (2009).
[2] N. Moiseyev, *Non-Hermitian Quantum Mechanics* (Cambridge University Press, Cambridge, England, 2011).
[3] D. C. Brody, J. Phys. A **47**, 035305 (2013).
[4] Y. Ashida, Z. Gong, and M. Ueda, Adv. Phys. **69**, 249 (2020).
[5] E. J. Bergholtz, J. C. Budich, and F. K. Kunst, Rev. Mod. Phys. **93**, 015005 (2021).
[6] K. Ding, C. Fang, and G. Ma, Nat. Rev. Phys. **4**, 745 (2022).
[7] A. Regensburger, C. Bersch, M.-A. Miri, G. Onishchukov, D. N. Christodoulides, and U. Peschel, Nature (London) **488**, 167 (2012).
[8] T. Gao, E. Estrecho, K. Y. Bliokh, T. C. H. Liew, M. D. Fraser, S. Brodbeck, M. Kamp, C. Schneider, S. Höfling, Y. Yamamoto, F. Nori, Y. S. Kivshar, A. G. Truscott, R. G. Dall, and E. A. Ostrovskaya, Nature (London) **526**, 554 (2015).
[9] L. Feng, R. El-Ganainy, and L. Ge, Nat. Photonics **11**, 752 (2017).
[10] M.-A. Miri and A. Alù, Science **363**, eaar7709 (2019).
[11] Ş. K. Özdemir, S. Rotter, F. Nori, and L. Yang, Nat. Mater. **18**, 783 (2019).
[12] C. Scheibner, A. Souslov, D. Banerjee, P. Surówka, W. T. M. Irvine, and V. Vitelli, Nat. Phys. **16**, 475 (2020).
[13] C. Scheibner, W. T. M. Irvine, and V. Vitelli, Phys. Rev. Lett. **125**, 118001 (2020).
[14] D. Zhou and J. Zhang, Phys. Rev. Res. **2**, 023173 (2020).
[15] H. Xiu, I. Frankel, H Liu, K. Qian, S. Sarkar, B. MacNider, Z. Chen, N. Boechler, and X. Mao, Proc. Natl. Acad. Sci. U.S.A. 2217928120 (2023).
[16] V. Kozii and L. Fu, arXiv:1708.05841.
[17] H. Shen and L. Fu, Phys. Rev. Lett. **121**, 026403 (2018).
[18] Y. Nagai, Y. Qi, H. Isobe, V. Kozii, and L. Fu, Phys. Rev. Lett. **125**, 227204 (2020).
[19] A. McDonald, T. Pereg-Barnea, and A. A. Clerk, Phys. Rev. X **8**, 041031 (2018).
[20] S. Yao and Z. Wang, Phys. Rev. Lett. **121**, 086803 (2018).
[21] F. K. Kunst, E. Edvardsson, J. C. Budich, and E. J. Bergholtz, Phys. Rev. Lett. **121**, 026808 (2018).
[22] S. Yao, F. Song, and Z. Wang, Phys. Rev. Lett. **121**, 136802 (2018).
[23] V. M. Martinez Alvarez, J. E. Barrios Vargas, and L. E. F. Foa Torres, Phys. Rev. B **97**, 121401(R) (2018).
[24] K. Yokomizo and S. Murakami, Phys. Rev. Lett. **123**, 066404 (2019).

[25] F. Song, S. Yao, and Z. Wang, Phys. Rev. Lett. **123**, 170401 (2019).
[26] K. Kawabata, K. Shiozaki, M. Ueda, and M. Sato, Phys. Rev. X **9**, 041015 (2019).
[27] C. H. Lee and R. Thomale, Phys. Rev. B **99**, 201103(R) (2019).
[28] C. H. Lee, L. Li, and J. Gong, Phys. Rev. Lett. **123**, 016805 (2019).
[29] J. Y. Lee, J. Ahn, H. Zhou, and A. Vishwanath, Phys. Rev. Lett. **123**, 206404 (2019).
[30] T. Liu, Y.-R. Zhang, Q. Ai, Z. Gong, K. Kawabata, M. Ueda, and F. Nori, Phys. Rev. Lett. **122**, 076801 (2019).
[31] T.-S. Deng and W. Yi, Phys. Rev. B **100**, 035102 (2019).
[32] S. Longhi, Phys. Rev. Res. **1**, 023013 (2019).
[33] K. Zhang, Z. Yang, and C. Fang, Phys. Rev. Lett. **125**, 126402 (2020).
[34] D. S. Borgnia, A. J. Kruchkov, and R.-J. Slager, Phys. Rev. Lett. **124**, 056802 (2020).
[35] N. Okuma, K. Kawabata, K. Shiozaki, and M. Sato, Phys. Rev. Lett. **124**, 086801 (2020).
[36] Z. Yang, K. Zhang, C. Fang, and J. Hu, Phys. Rev. Lett. **125**, 226402 (2020).
[37] Y. Yi and Z. Yang, Phys. Rev. Lett. **125**, 186802 (2020).
[38] T. Hofmann, T. Helbig, F. Schindler, N. Salgo, M. Brzezińska, M. Greiter, T. Kiessling, D. Wolf, A. Vollhardt, A. Kabaši, C. H. Lee, A. Bilušić, R. Thomale, and T. Neupert, Phys. Rev. Res. **2**, 023265 (2020).
[39] M. M. Denner, A. Skurativska, F. Schindler, M. H. Fischer, R. Thomale, T. Bzdušek, and T. Neupert, Nat. Commun. **12**, 5681 (2021).
[40] K. Kawabata, M. Sato, and K. Shiozaki, Phys. Rev. B **102**, 205118 (2020).
[41] L. Li, C. H. Lee, and J. Gong, Phys. Rev. Lett. **124**, 250402 (2020).
[42] L. Li, C. H. Lee, S. Mu, and J. Gong, Nat. Commun. **11**, 5491 (2020).
[43] C.-H. Liu, K. Zhang, Z. Yang, and S. Chen, Phys. Rev. Res. **2**, 043167 (2020).
[44] K. Kawabata, N. Okuma, and M. Sato, Phys. Rev. B **101**, 195147 (2020).
[45] T. Helbig, T. Hofmann, S. Imhof, M. Abdelghany, T. Kiessling, L. W. Molenkamp, C. H. Lee, A. Szameit, M. Greiter, and R. Thomale, Nat. Phys. **16**, 747 (2020).
[46] A. Ghatak, M. Brandenbourger, J. van Wezel, and C. Coulais, Proc. Natl. Acad. Sci. U.S.A. **117**, 29561 (2020).
[47] L. Xiao, T. Deng, K. Wang, G. Zhu, Z. Wang, W. Yi, and P. Xue, Nat. Phys. **16**, 761 (2020).
[48] W.-T. Xue, M.-R. Li, Y.-M. Hu, F. Song, and Z. Wang, Phys. Rev. B **103**, L241408 (2021).
[49] X.-Q. Sun, P. Zhu, and T. L. Hughes, Phys. Rev. Lett. **127**, 066401 (2021).
[50] K. Kawabata, K. Shiozaki, and S. Ryu, Phys. Rev. Lett. **126**, 216405 (2021).
[51] T. Bessho and M. Sato, Phys. Rev. Lett. **127**, 196404 (2021).
[52] L. Li, S. Mu, C. H. Lee, and J. Gong, Nat. Commun. **12**, 5294 (2021).
[53] Y. Liu, Y. Wang, X.-J. Liu, Q. Zhou, and S. Chen, Phys. Rev. B **103**, 014203 (2021).
[54] C.-X. Guo, C.-H. Liu, X.-M. Zhao, Y. Liu, and S. Chen, Phys. Rev. Lett. **127**, 116801 (2021).
[55] M. Lu, X.-X. Zhang, and M. Franz, Phys. Rev. Lett. **127**, 256402 (2021).
[56] L. Mao, T. Deng, and P. Zhang, Phys. Rev. B **104**, 125435 (2021).
[57] F. Song, H.-Y. Wang, and Z. Wang, Non-Bloch PT symmetry: Universal threshold and dimensional surprise, in *A Festschrift in Honor of the C. N. Yang Centenary* (World Scientific, 2022), pp. 299–311.
[58] K. Zhang, Z. Yang, and C. Fang, Nat. Commun. **13**, 2496 (2022).
[59] Z. Fang, M. Hu, L. Zhou, and K. Ding, Nanophotonics **11**, 3447 (2022).
[60] Y.-C. Wang, J.-S. You, and H. H. Jen, Nat. Commun. **13**, 4598 (2022).
[61] S. Longhi, Phys. Rev. Lett. **128**, 157601 (2022).
[62] S. Longhi and E. Pinotti, Phys. Rev. B **106**, 094205 (2022).
[63] Q. Liang, D. Xie, Z. Dong, H. Li, H. Li, B. Gadway, W. Yi, and B. Yan, Phys. Rev. Lett. **129**, 070401 (2022).
[64] H. Geng, J. Y. Wei, M. H. Zou, L. Sheng, W. Chen, and D. Y. Xing, Phys. Rev. B **107**, 035306 (2023).
[65] H. Jiang and C. H. Lee, arXiv:2207.08843.
[66] K. Yokomizo and S. Murakami, Phys. Rev. B **107**, 195112 (2023).
[67] H.-Y. Wang, F. Song, and Z. Wang, arXiv:2212.11743.
[68] H. Zhou, C. Peng, Y. Yoon, C. W. Hsu, K. A. Nelson, L. Fu, J. D. Joannopoulos, M. Soljačić, and B. Zhen, Science **359**, 1009 (2018).
[69] B. Lv, T. Qian, and H. Ding, Nat. Rev. Phys. **1**, 609 (2019).
[70] See Supplemental Material at http://link.aps.org/supplemental/10.1103/PhysRevLett.131.036402 for (i) equal frequency contour and dynamical degeneracy splitting; (ii) scattering theory in the non-Hermitian tight-binding Hamiltonian; (iii) analysis of the time evolution of scattering waves; (iv) the relation between directional invisibility and geometry-dependent skin effect; (v) the robustness of anomalous scattering.